European Radiology (2022) 32:6910–6921
https://doi.org/10.1007/s00330-022-08853-w

HEAD AND NECK

A MRI-based radiomics model predicting radiation-induced temporal lobe injury in nasopharyngeal carcinoma

Dan Bao[1] · Yanfeng Zhao[1] · Lin Li[1] · Meng Lin[1] · Zheng Zhu[1] · Meng Yuan[2] · Hongxia Zhong[1] · Haijun Xu[1] · Xinming Zhao[1] · Dehong Luo[1,3]

Received: 26 February 2022 / Revised: 26 April 2022 / Accepted: 28 April 2022 / Published online: 31 May 2022

Abstract

Objectives To develop and validate a radiomics-based model for predicting radiation-induced temporal lobe injury (RTLI) in nasopharyngeal carcinoma (NPC) by pretreatment MRI of the temporal lobe.

Methods A total of 216 patients with diagnosed NPC were retrospectively reviewed. Patients were randomly allocated to the training ($n = 136$) and the validation cohort ($n = 80$). Radiomics features were extracted from pretreatment contrast-enhanced T1- or fat-suppressed T2 weighted MRI. A radiomics signature was generated by the least absolute shrinkage and selection operator (LASSO) regression algorithm, Pearson correlation analysis, and univariable logistic analysis. Clinical features were selected with logistic regression analysis. Multivariable logistic regression analysis was conducted to develop three models for RTLI prediction in the training cohort: namely radiomics signature, clinical variables, and clinical-radiomics parameters. A radiomics nomogram was used and assessed with respect to calibration, discrimination, reclassification, and clinical application.

Results The radiomics signature, composed of two radiomics features, was significantly associated with RTLI. The proposed radiomics model demonstrated favorable discrimination in both the training (AUC, 0.89) and the validation cohort (AUC, 0.92), outperforming the clinical prediction model ($p < 0.05$). Combining radiomics and clinical features, higher AUCs were achieved (AUC, 0.93 and 0.95), as well as a better calibration and improved accuracy of the prediction of RTLI. The clinical-radiomics model showed also excellent performance in predicting RTLI in different clinical-pathologic subgroups.

Conclusion A radiomics model derived from pretreatment MRI of the temporal lobe showed persuasive performance for predicting radiation-induced temporal lobe injury in nasopharyngeal carcinoma.

Key Points

- *Radiomics features from pretreatment MRI are associated with radiation-induced temporal lobe injury in nasopharyngeal carcinoma.*
- *The radiomics model shows better predictive performance than a clinical model and was similar to a clinical-radiomics model.*
- *A clinical-radiomics model shows excellent performance in the prediction of radiation-induced temporal lobe injury in different clinical-pathologic subgroups.*

Keywords Nasopharyngeal carcinoma · Temporal lobe · Radiation · Radiomics · Magnetic resonance imaging

Yanfeng Zhao and Dehong Luo contributed equally to this work as corresponding authors.

✉ Yanfeng Zhao
zyf24@sina.com

✉ Dehong Luo
cjr.luodehong@vip.163.com

[1] Department of Radiology, National Cancer Center/National Clinical Research Center for Cancer/Cancer Hospital, Chinese Academy of Medical Sciences and Peking Union Medical College, 17 Panjiayuan Nanli, Chaoyang District, Beijing 100021, China

[2] Department of Radiation Oncology, National Cancer Center/National Clinical Research Center for Cancer/Cancer Hospital, Chinese Academy of Medical Sciences and Peking Union Medical College, 17 Panjiayuan Nanli, Chaoyang District, Beijing 100021, China

[3] Department of Radiology, National Cancer Center/National Clinical Research Center for Cancer/Cancer Hospital & Shenzhen Hospital, Chinese Academy of Medical Sciences and Peking Union Medical College, Shenzhen 518116, China

Abbreviations

AUC	Area under the curve
IMRT	Intensity-modulated radiotherapy
NPC	Nasopharyngeal carcinoma
ROI	Region of interest
RTLI	Radiotherapy-induced temporal lobe injury
TL	Temporal lobe
VOI	Volume of interests

Introduction

Nasopharyngeal carcinoma (NPC) is a very common endemic neoplasm in southeast and eastern Asia [1]. Radiotherapy is currently the preferred modality of treatment for non-metastatic NPC, but the temporal lobes (TL) are inevitably included in the radiation field [2, 3]. The reported rate of radiation-induced temporal lobe injury (RTLI) ranges from 4.6 to 8.5% for patients treated with intensity-modulated radiation therapy (IMRT) radiotherapy [4–6]. Patients who developed RTLI suffer damages in memory, language, and mobility [7], but nearly half of the patients (45.3%) are asymptomatic for RTLI on diagnosis [7] and the majority of patients were asymptomatic even at a late stage [8]. The early identification or individualized prediction of RTLI is an important requirement for improving the quality of life and prognosis in NPC patients [9].

Some studies focused on identifying the risk factors leading to RTLI. Guan [10] developed a model for the prediction of RTLI in NPC patients including D_{max} (the maximum point dose) of the TL, D_{1cc} (the maximum dose delivered to a 1-cm^3 volume), T stage, and neutrophil-to-lymphocyte ratios (NLRs). Zeng [11] and Huang [12] reported that D_{1cc} and V_{20} (absolute volumes of the TL receiving at least 20 Gy) were predictive of RTLI for NPC. However, the optimal dose/volume predictors for RTLI still vary in different studies and the clinical application is limited. The imaging diagnosis of RTLI mainly depends on MRI currently [13]. However, existing conventional MRI techniques can only differentiate RTLI at the irreversible stage [14]. Other advanced imaging modalities, such as diffusion and perfusion MRI, have been reported to provide additional information in RTLI diagnosis [15, 16]. But functional MRI has higher requirements for equipment and scanning technology. Considering the long latency period and few cases of RTLI, it is very challenging to guarantee the accuracy and consistency of the predefined region of interest (ROI) placements; otherwise, it will introduce great variation in the measuring results and lead to inconsistent conclusions. Recently, artificial intelligence (AI) such as radiomics has been widely used in predicting treatment effects such as complications and disease progression [17]. Radiomics describes the process of extracting large amounts of image-based features from routine diagnostic scans. High-dimensional data that quantify tumor shape, image intensity, and texture may reflect the characteristics of the disease, which can be applied within clinical decision support [18].

The purpose of this study is to develop and validate a radiomics-based model for the pretreatment prediction of RTLI in patients with NPC.

Materials and methods

Patient selection

The institutional review board approved this retrospective study, and the requirement to obtain informed consent was waived (institutional ethics approval number 21/278-2949). We searched the radiology reports for the term radiation-induced temporal lobe injury on MRI scans obtained between January 2017 and May 2021. A total of 108 NPC patients of RTLI were included according to the inclusion and exclusion criteria (Fig. 1; Supplementary Text). The 108 controls were randomly selected from patients without RTLI after IMRT between January 2017 and May 2021 according to the inclusion and exclusion criteria (Fig. 1; Supplementary Text). Thus, 216 patients were included in this study, which were randomly allocated to a training set (136 patients) and a validation set (80 patients).

Baseline clinical-pathologic data, including gender, age, NLRs, stage (T stage, N stage, and clinical stage), pathologic type, treatment, D_{max} for each TL, and the planning gross tumor volume included the primary nasopharyngeal tumor or enlarged retropharyngeal nodes ($PGTV_{NX}$) were obtained from the medical records. All patients underwent a standard treatment regimen that consisted of IMRT and concurrent or adjuvant chemotherapy with or without induction. IMRT was performed with a total dose of 70–76 Gy and took 30–33 times to complete. After completion of radiation therapy, follow-up MRI of the head and neck was performed every 1–3 months during the first 2 years, every 6 months in years 3–5, and annually thereafter [2]. Diagnostic criteria for temporal lobe injury [19] were as follows: (a) white matter lesions, defined as areas of finger-like lesions of increased signal intensity on T2-weighted images; (b) contrast-enhanced lesions, defined as lesions with or without necrosis on post-contrast T1-weighted images with heterogeneous signal abnormalities on T2-weighted images; (c) cysts, round or oval well-defined lesions of very high signal intensity on T2-weighted images with a thin or imperceptible wall.

Image acquisition

MRI examinations were performed by using 3.0-T scanner (GE Discovery MR 750, General Electric Medical Systems)

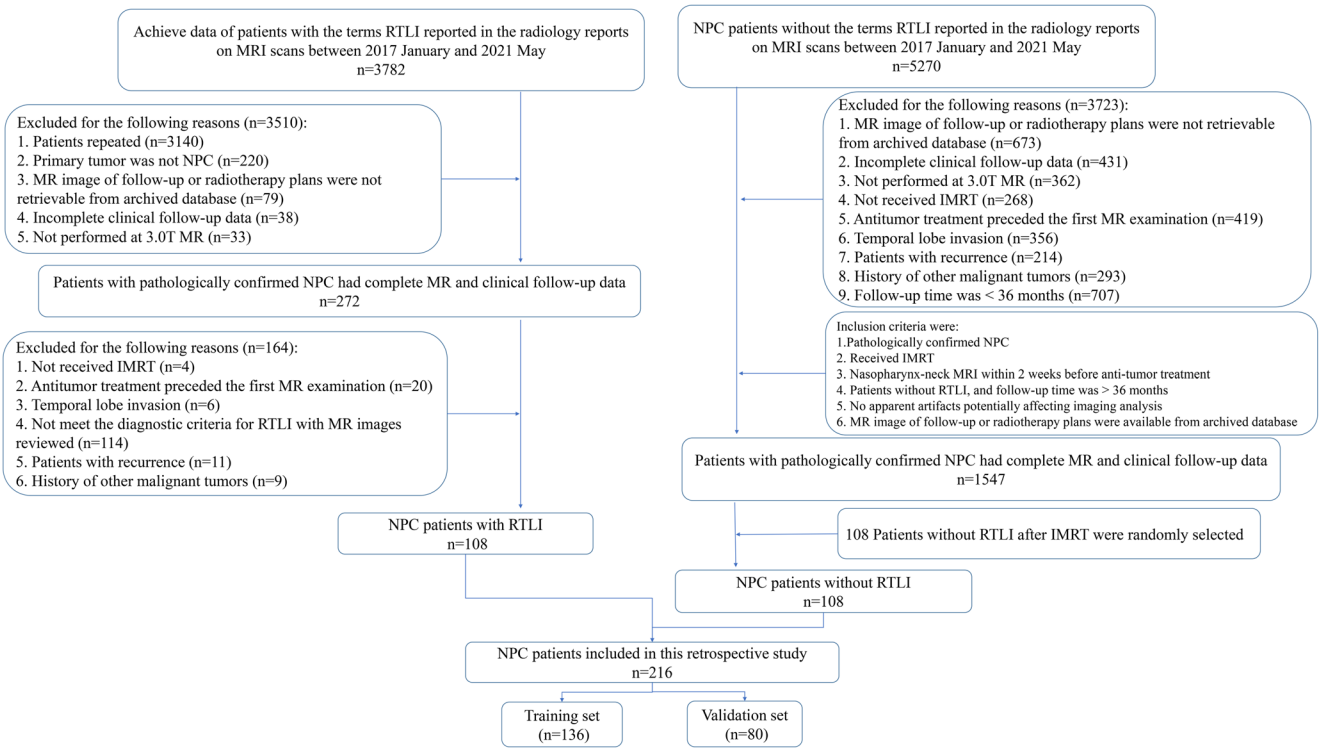

Fig. 1 Diagram for inclusion of patients into the study. IMRT intensity-modulated radiotherapy, NPC nasopharyngeal carcinoma, RTLI radiation-induced temporal lobe injury

with an 8-channel head and neck phased array coil. Axial fast spoiled gradient-echo (FSPGR) contrast-enhanced T1-weighted (CE-T1w) imaging was performed 60 s after intravenous bolus injection of gadopentetate dimeglumine (Magnevist, Bayer, Leverkusen) at a dosage of 0.2 ml/kg of body weight and 1.5 ml/s using a power injector. The imaging protocol with parameters used is detailed in Supplementary Table 1.

Temporal lobe segmentation

Axial fat-suppressed T2-weighted (FS-T2w) and CE-T1w MR images were loaded into ITK-SNAP software (version 3.6.0, http://www.itksnap.org) for segmentation. The ROI was manually delineated along the boundaries of the middle and lower portions of the TL, from the top level of the cerebral peduncle to the bottom of the TL. Bilateral temporal lobes were covered in the ROI of all patients. All segmentations were performed by one radiologist (D.B., with 5 years of experience in head and neck MRI diagnosis) and confirmed by another senior radiologist (D.H.L., with 38 years of experience). Disagreements were resolved by consensus. To assess for segmentation variability, a subset of 30 randomly selected patients was independently delineated by one radiologist (Y.F.Z., with 19 years of experience). The reliability was calculated by using the Dice similarity coefficient (DSC). According to the guidelines [20], DSC ≥ 0.75 indicates good agreement.

Radiomics feature extraction

Radiomic features were extracted from the volume of interests (VOIs) by using the AK software (Analysis Kit, GE Healthcare). MR images were normalized by centering to the mean standard deviation, resampled to a voxel size of 1 × 1 × 1 mm^3 using B-Spline interpolation with gray-level discretized by a fixed bin width of 25 in the histogram. In total, 1316 radiomics features including 14 shape features, 252 first-order intensity features, and 1050 texture features were extracted from each sequence.

Feature selection and signature construction

We devised a three-step procedure for dimensionality reduction and selection of robust features (Fig. 2). First, the least absolute shrinkage and selection operator (LASSO) regression was performed to reduce irrelevant features in the training set. Pearson correlation analysis was used to further reduce the redundancy of radiomic features with one of the paired significantly correlated features ($p < 0.05$ and correlation coefficient > 0.5)

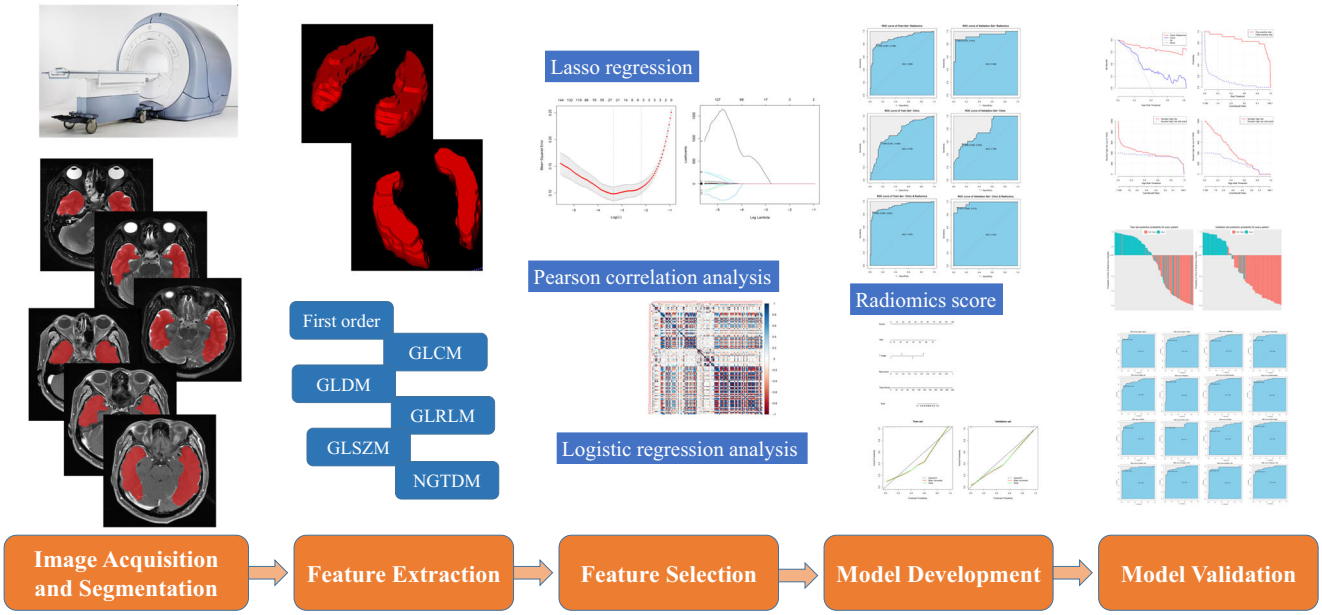

Fig. 2 Workflow of the development and testing of a radiomics model. GLCM gray level co-occurrence matrix, GLDM gray level dependence matrix, GLRLM gray level run length matrix, GLSZM gray level size zone matrix, NGTDM neighboring gray tone difference matrix

removed from further analysis. Finally, multivariable logistic analysis was applied to select RTLI-related features with $p < 0.05$. A radiomics signature (Rad-score) was generated via a linear combination of selected features weighted by their respective coefficients. The association of clinical variables with RTLI was evaluated by using logistic regression analysis.

Model development and validation

Logistic regression analysis was conducted to develop three models for RTLI prediction in the training cohort: including radiomics signature, clinical variables, and clinical-radiomics parameters, respectively. A function on the basis of the variance inflation factor was conducted to check for the collinearity of variables included in the regression equations. A variance inflation fact factor greater than 10 indicates multicollinearity [21]. The predictive performance of established models was quantified by the receiver operating characteristic (ROC) curve and the area under the curve (AUC). AUC estimates were compared between prediction models by using the Delong nonparametric approach. Tenfold cross-validation was performed with iteration of model development. The average AUC and average sensitivity, specificity, and accuracy were provided as performance metrics. To provide a more understandable outcome measure, a nomogram was then constructed. Calibration curves were plotted via bootstrapping with 1000 resamples to assess the calibration of the radiomics model, accompanied by the Hosmer-Lemeshow goodness-of-fit test. Decision curve analysis (DCA) was used to calculate the net benefit from the use of the radiomics model at different threshold probabilities in the validation dataset. Patients were classified into high-risk or low-risk groups according to the clinical-radiomics model, and the threshold was identified by using ROC with the AUC analysis. The predictive ability of the model in subgroups with different clinical-pathologic characteristics was assessed with ROC analysis.

Statistical analysis

Categorical variables were compared by x^2 test or Fisher exact test. Continuous variables were compared by independent samples t-test or Mann-Whitney U test. Statistical analysis was performed by using SPSS 26.0 (IBM) and R software (version 3.4.4, www.r-project.org). A two-sided p value less than 0.05 was considered to indicate statistical significance. The packages in R used in this study are described in Supplementary Table 2.

Results

Patient demographics

A total of 216 patients, including 145 men (mean age, 47.2 years; age range, 10–73 years) and 71 women (mean age, 44.1 years; age range, 9–65 years), were identified

Table 1 Characteristics of patients in the training and validation cohorts

Characteristic	Training cohort (n = 156)	Validation cohort (n = 60)	p value
Age (y)*	46.01 ± 13.23 (9–73)	46.53 ± 12.20 (19–69)	0.78
Gender			
Male	88	57	0.32
Female	48	23	
NLRs (mean ± SD) *	3.40 ± 4.54 (0.43–48.63)	3.14 ± 1.80 (0.86–12.29)	0.63
T stage			0.65
T1	6	6	
T2	11	4	
T3	67	41	
T4	52	29	
N stage			0.89
N0	18	8	
N1	50	29	
N2	51	33	
N3	17	10	
TNM stage			0.93
I	0	2	
II	8	2	
III	65	37	
IV	63	39	
Pathology			0.40
Differentiated	50	34	
Undifferentiated	86	46	
Synchronous chemotherapy			0.91
Yes	101	60	
No	35	20	
Targeted therapy			0.58
Yes	51	27	
No	85	53	
Induction chemotherapy			0.82
Yes	29	16	
No	107	64	
$PGTV_{nx}$ (mean ± SD)(Gy) *	73.52 ± 1.24 (67.72–74.20)	73.72 ± 0.87 (69.96–73.92)	0.19
LD_{max} (mean ± SD) (Gy) *	68.12 ± 5.90 (54.90–86.07)	68.35 ± 5.63 (52.86–77.99)	0.78
RD_{max} (mean ± SD) (Gy) *	68.98 ± 5.65 (55.16–86.07)	68.23 ± 5.17 (55.93–78.80)	0.33

Note. — *Data are mean ± standard deviation; data in parentheses are range. $p > 0.05$ suggests no significant difference between the subjects in the two cohorts. LD_{max} maximum dose of the left temporal lobe, *NLRs* neutrophil-to-lymphocyte ratios, $PGTV_{NX}$ planning gross tumor volume included the primary nasopharyngeal tumor or enlarged retropharyngeal nodes, RD_{max} maximum dose of the right temporal lobe, *TNM* tumor-node-metastasis

according to the inclusion and exclusion criteria (Fig. 1; Supplementary Text). Clinical characteristics of the training (n = 136) and validation (n = 80) sets are summarized in Table 1. There were no differences in clinical characteristics between the training and validation cohorts. Baseline clinical characteristics in patients with and without RTLI are summarized in Supplementary Table 3. 108 patients included in the present study were diagnosed with RTLI (bilateral, 23; left, 39; right, 46). The ratio of RTLI was 56.88% (76 of 136) and 24.12% (32 of 80) in the training and validation cohorts, respectively. The median duration of follow-up was 33.3 months (interquartile range, 25.8–41.9 months) until RTLI and 61.0 months (interquartile range, 53.2–66.7 months) without RTLI.

Table 2 Risk factors for radiation-induced temporal lobe injury of nasopharyngeal carcinoma in the training cohort

Variable	β	SE	Wald	P	OR	95%CI	
						Lower	Upper
Age	0.06	0.02	7.22	0.007*	1.07	1.02	1.12
T stage	1.26	0.44	8.39	0.004*	3.53	1.59	8.98
NGTDM	33539.33	6282.78	28.50	< 0.001*	Inf	Inf	Inf
GLSZM	18.46	8.49	4.72	0.03*	1.04e+08	20.73	5.7e+15

Note.—Data are results of the multivariable regression analysis. *CI* confidence interval, *GLSZM* CET1w_wavelet-HHH_glszm_SmallAreaEmphasis, *Inf* infinity, *NGTDM* T2w_lbp-3D-k_ngtdm_Strength, *OR* odds ratio, *SE* standard error. * indicates significant difference

Inter-observer reproducibility variability of segmentation

The intra-reader Dice value was 0.98 ± 0.002 (range 0.978–0.985) for FS-T2w sequences and 0.98 ± 0.002 (range 0.977–0.985) for CE-T1w sequences between the two radiologists. These results indicated a favorable inter-observer reproducibility for manual segmentation.

Feature selection and radiomics signature construction

Among 2632 extracted radiomics features from both FS-T2w and CE-T1w images, 120 features associated with RTLI in the LASSO regression algorithm were identified.

Table 3 Predictive performances of three models in predicting the radiation-induced temporal lobe injury in the training and validation cohort

Model	AUC	95%CI		Sensitivity	Specificity
		Lower	Upper		
Radiomic and clinical					
Training cohort	0.93	0.88	0.97	0.79 (60/76)	0.98 (59/60)
Validation cohort	0.95	0.90	1.00	0.81 (26/32)	0.96 (46/48)
Radiomics only*					
Training cohort	0.89	0.83	0.94	0.75 (57/76)	0.95 (57/60)
Validation cohort	0.92	0.85	0.99	0.66 (21/32)	0.96 (46/48)
Clinical only					
Training cohort	0.74	0.65	0.82	0.59 (45/76)	0.87 (52/60)
Validation cohort	0.77	0.66	0.87	0.59 (19/32)	0.71 (34/48)

AUC area under the receiver operating characteristic curve, *CI* confidence interval

*Features used for the radiomics-only model are FS/T2w-lbp-3D-k_ngtdm_Strength and CET1w- wavelet-HHH_glszm_SmallAreaEmphasis

Features used for the clinical-only model are T stage and age

The Pearson correlation analysis was then used to select 11 features for subsequent analysis. The 11 radiomics variables in patients with and without RTLI are summarized in Supplementary Table 3. The 2 most relevant and stable features (one ngtdm and one glszm feature) from the training set were selected. The radiomics signature was constructed, with a Rad-score calculated by using the following formula:

$$log(radiomics\ score) = -15.34 + 31876.46 \times T2\text{-}W\_ngtdm\_strength + 16.38 \times CET1\text{-}W\_glszm\_Small\ Area\ Emphasis$$

where ngtdm quantifies the difference between a gray value and the average gray value of its neighbors within distance δ, and glszm is the amount of homogeneous connected areas within the volume of a certain size and intensity.

Prediction model development and validation

The radiomics signature indicated a favorable prediction of RTLI with an AUC of 0.89 (95% confidence interval [CI]: 0.83–0.94) in the training cohort and 0.92 (95% CI:0.85–0.99) in the validation cohort. In the training cohort, 2 clinical variables (age, p = 0.01; T stage, $p < 0.001$) were predictive of RTLI in multivariable analysis. A clinical prediction model was built based on the two independent predictors without

Fig. 3 Performances of three models in training cohort and validation cohort. **a**, **b** Radiomics model, including two radiomics features- FS/T2w-lbp-3D-k_ngtdm_Strength and CET1w- wavelet-HHH_glszm_SmallAreaEmphasis. **c**, **d** Clinical model, including two clinical variables- T stage and age. **e**, **f** Clinical-radiomics radiomics, integrated two clinical variables and two radiomics features. ROC receiver operating characteristic curve

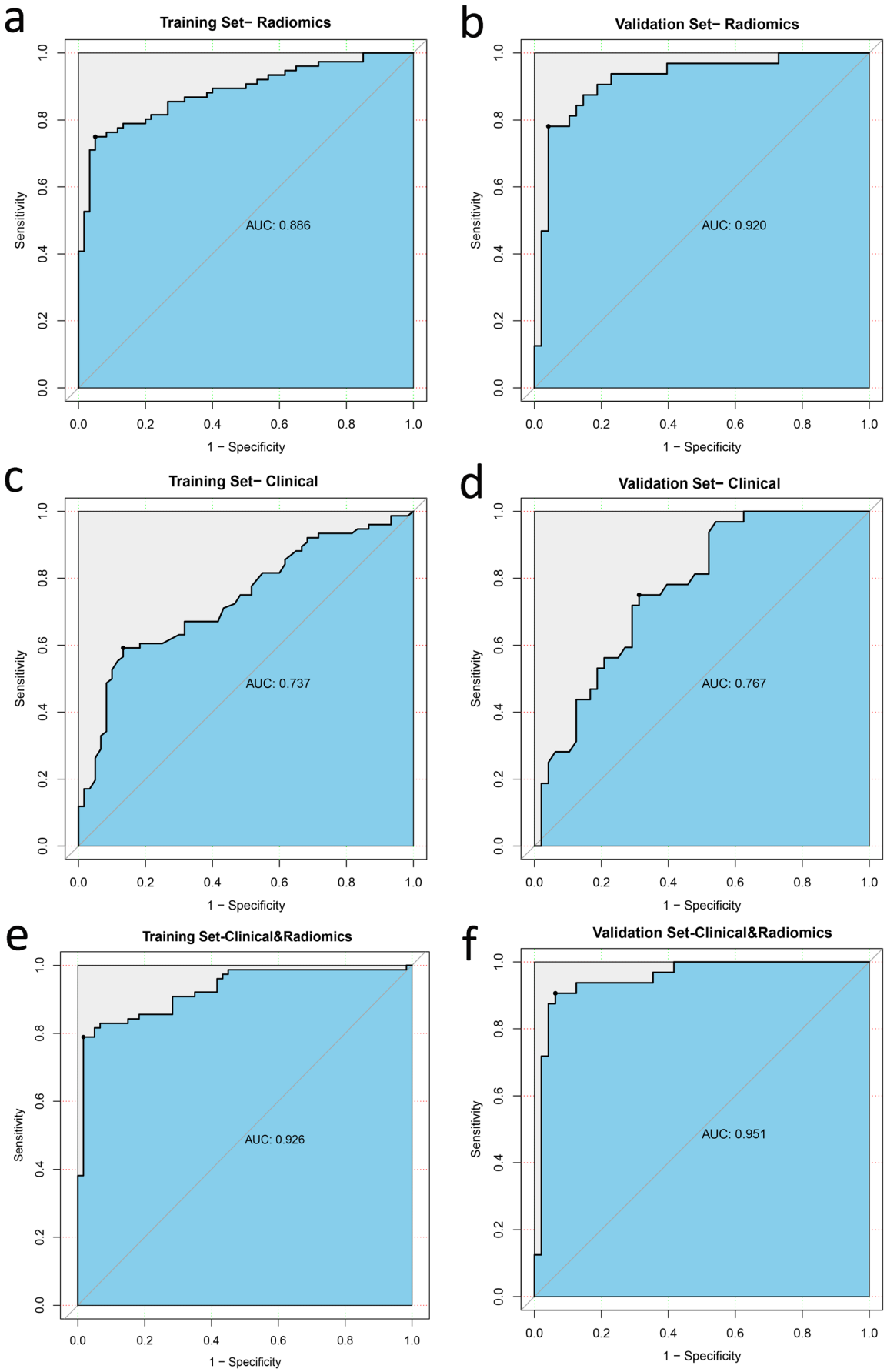
a
Training Set– Radiomics
AUC: 0.886
b
Validation Set– Radiomics
AUC: 0.920
c
Training Set– Clinical
AUC: 0.737
d
Validation Set– Clinical
AUC: 0.767
e
Training Set-Clinical&Radiomics
AUC: 0.926
f
Validation Set-Clinical&Radiomics
AUC: 0.951
Sensitivity
1 – Specificity
0.0
0.2
0.4
0.6
0.8
1.0

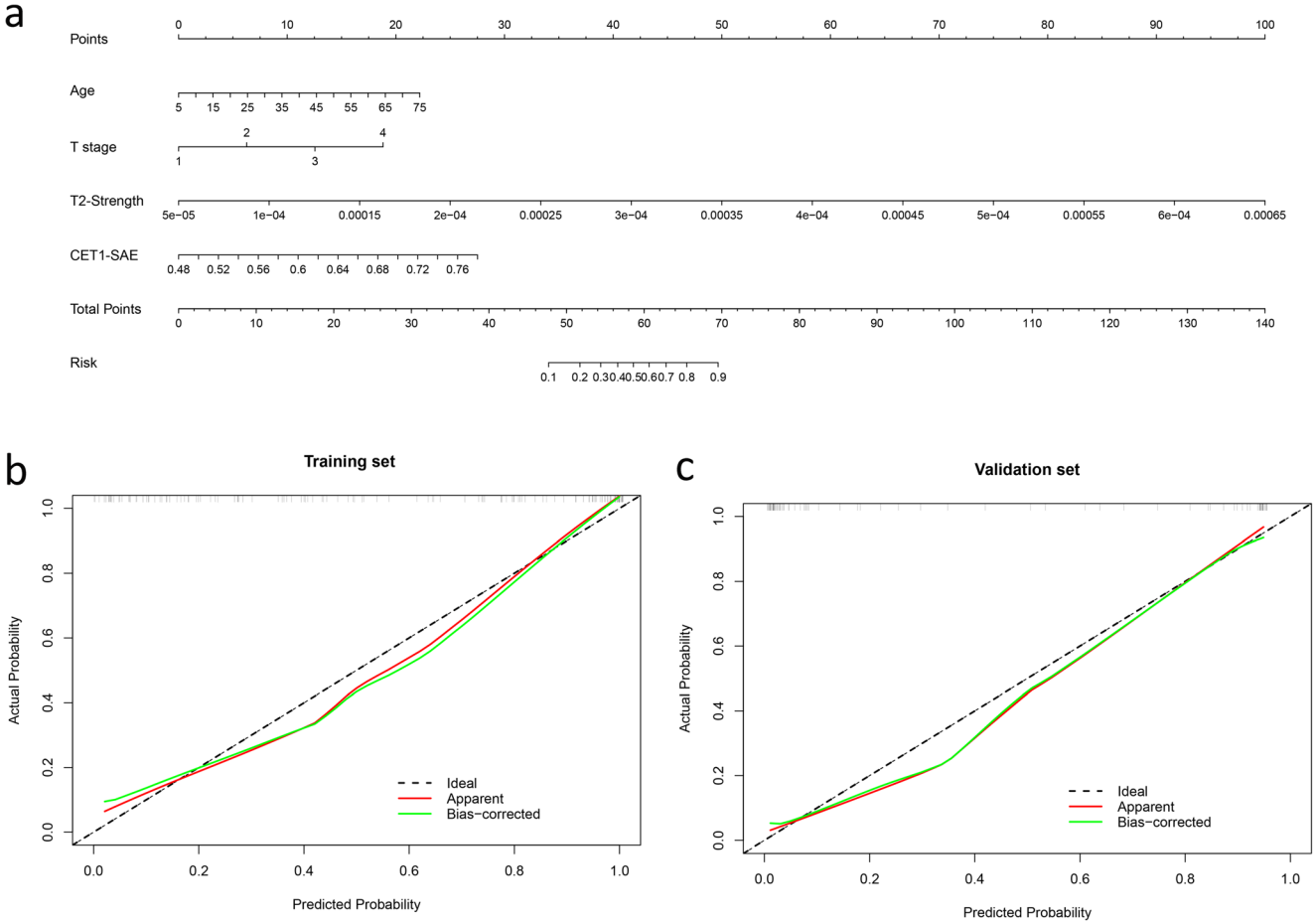

Fig. 4 Radiomics nomogram developed with receiver operating characteristic curves and calibration curves. **a** A radiomics nomogram was constructed in the training cohort, with radiomics score, T stage and age incorporated. Calibration curves of the radiomics nomogram in the (**b**) training and (**c**) validation cohorts. CET1-SAE CET1w_wavelet-HHH_glszm_SmallAreaEmphasis, T2-Strength T2w_lbp-3D-k_ngtdm_Strength

the addition of a radiomics signature. With the use of multivariable logistic regression analysis, independent predictors were identified for the clinical-radiomics model (Table 2). The variance inflation factors of the four potential predictors ranged from 1.039 to 1.081, indicating no multicollinearity. The AUCs of the clinical-radiomics model for predicting RTLI in the training and validation cohorts were 0.93 (95% CI: 0.88–0.97) and 0.95 (95% CI: 0.90–1.00), respectively. The AUC value of the clinical-radiomics model was higher than that of the radiomics model, but the difference was not statistically significant (p = 0.09) in the validation cohort, while the radiomics model was significantly better than the clinical model in the prediction of RTLI (p = 0.02) (Table 3 and Fig. 3).

A nomogram integrating Rad-Score and two clinical features was constructed (Fig. 4a). The calibration curve of the clinical-radiomics nomogram demonstrated good agreement between predicted and observed RTLI in both the training and validation cohorts (Fig. 4b, c). No significant difference was found in the Hosmer–Lemeshow test (p = 0.08), suggesting no departure from the good fit. The DCA showed that the radiomics signature and the clinical-radiomics model provide a better net benefit to predict RTLI than the clinical model across the majority of the range of reasonable threshold probabilities (Fig. 5).

The optimum cutoff of the clinical-radiomics model was generated by the ROC analysis with the AUC equals 0.732 from the training cohort. The average AUC of the clinical-radiomics model from 10-fold cross-validation was 0.93 (sensitivity, 97%; specificity, 70%; and accuracy, 83%) with a threshold probability of 0.732. Accordingly, patients were classified into a high-risk group (Rad-score ≥ 0.732) and a low-risk group (Rad-score < 0.732). When assessing the distribution of risk value and RTLI status, patients with lower risk values generally had a lower probability of RTLI than higher risk values (Supplementary Fig. 1). When the patients were stratified based on clinical-pathologic factors,

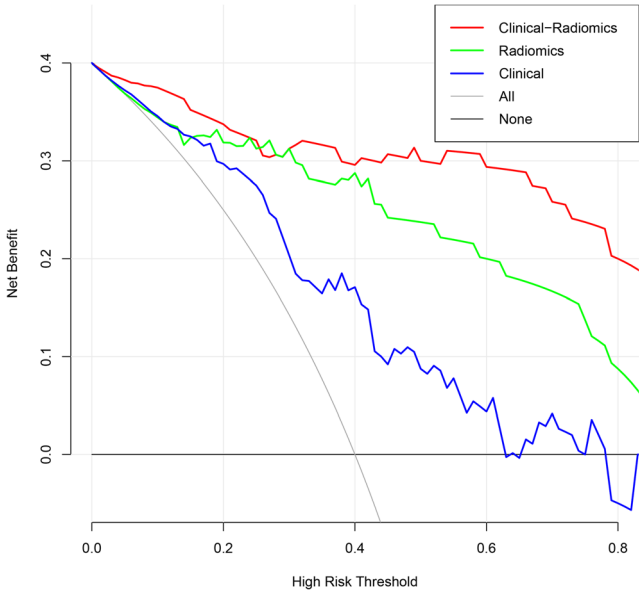

Fig. 5 Decision curve analysis for each model in the validation dataset. The y-axis measures the net benefit, which is calculated by summing the benefits (true-positive findings) and subtracting the harms (false-positive findings), weighting the latter by a factor related to the relative harm of undetected radiation-induced temporal lobe injury (RTLI) compared with the harm of unnecessary treatment

an excellent predictive performance of the clinical-radiomics model was found in all subgroups (AUC = 0.88–0.97) (Table 4 and Fig. 6).

Discussion

In this study, we developed and validated a radiomics model to evaluate the prediction of nasopharyngeal carcinoma (NPC) patients at risk of radiation-induced temporal lobe injury (RTLI) by radiomics features which are extracted from pretreatment MRI of the temporal lobe. The radiomics model demonstrated excellent predictive performance with the validation set (AUC, 0.92; sensitivity, 66%; specificity, 96%). The clinical-radiomics model showed excellent predictive performance of RTLI in patients within different clinical-pathologic subgroups, thereby may facilitate pretreatment discrimination of NPC patients at high risk for RTLI.

The RTLI-related radiomics features with the maximum significance in the present study were "lbp-3D-k_ngtdm_Strength" and "wavelet-HHH_glszm_SmallAreaEmphasis," which were extracted from FS-T2w and CE-T1w images respectively. The precise mechanism that leads to RTLI and the association with TL heterogeneity remains unknown and is rarely investigated currently. SmallAreaEmphasis (SAE) measures the distribution of small size zones, with a greater value indicative of smaller size zones and more fine textures [22]. Strength is a measure of the primitives in an image, and its value is high when the primitives are easily defined and visible [23]. High values of SAE and strength in our study, increasing the radiomic score, were found to be associated with patients more prone to develop RTLI. SAE with a greater value indicates the minor difference between the gray-level values, and the higher value of strength is associated with an image with a slow change in intensity, indicating less heterogeneity of image textures [22–24]. This corresponded to the abundance of cells in the VOI of TL, with the cells arranged tightly and regularly. Furthermore, abundant blood supply and high oxygen demand of the corresponding TL, which means more sensitivity to radiotherapy [25, 26], thus more prone to develop RTLI [27]. Thus, our study demonstrated that this radiomics model could predict RTLI more accurately with an AUC of 0.89 in the training cohort and 0.92 in the validation cohort.

Our study focuses on the pretreatment MR images of NPC patients, enables early identification of RTLI, and provides the earliest prevention or protective personalized clinical treatment. Unlike the previous study that only included T2w sequence [28], CET1-w images were also included in our study. Some studies reported that the histological heterogeneity and structural changes associated with RTLI may be related to contrast enhancement [19, 29, 30]. Our result that the radiomics features finally selected were derived from both FS-T2w and CE-T1w images was consistent with it. Although the most frequent component of radiation-induced injury identified in some studies was white matter lesion, there were still some patients with extensive damage [31]. Therefore, the TL VOI we delineated not only included white matter, and this segmentation of the whole TL was more convenient and practical.

T stage and age were also found to be significant indicators of RTLI risk in the clinical model, which were consistent with previous studies [10, 28]. In clinical treatment, physicians have more interests in the clinical applications of AI models or comparison with clinical impact factors [32]. The clinical-radiomics model in our study successfully identified high-risk patients with RTLI, for whom earlier preventive treatment was recommended. The ability of radiomics features to help predict RTLI when the patients were stratified based on clinical-pathologic factors was evaluated and excellent predictive performances of the clinical-radiomics model were found in all subgroups.

Table 4 Diagnostic performance of clinical-radiomics model within different clinical-pathologic subgroups

Feature type and group	No. of patients	Diagnostic performance*	95%CI	
			Lower	Upper
Gender				
Male	145	0.92	0.87	0.97
Female	71	0.97	0.93	1.00
Age				
< 40	56	0.95	0.89	1.00
≥ 40	160	0.93	0.88	0.97
TNM stage				
I–III	135	0.89	0.82	0.96
IV	81	0.96	0.93	1.00
Pathology				
Differentiated	84	0.94	0.89	0.99
Undifferentiated	132	0.93	0.88	0.98
Synchronous chemotherapy				
Yes	161	0.94	0.91	0.98
No	55	0.91	0.83	0.99
Targeted therapy				
Yes	78	0.88	0.80	0.96
No	138	0.96	0.92	0.99
LD_{max}				
< 68	101	0.93	0.87	0.98
≥ 68	115	0.94	0.89	0.98
RD_{max}				
< 68	88	0.91	0.84	0.99
≥ 68	128	0.95	0.91	0.98

Note.—* Data are numbers of AUC. *CI* confidence interval, LD_{max} maximum dose of the left temporal lobe, RD_{max} maximum dose of the right temporal lobe, *TNM* tumor-node-metastasis

Our study had several limitations. Firstly, this study was retrospective with possible selection bias. The included patients without RTLI after IMRT were randomly selected. Although the preferred design should include all patients to ensure that no bias is introduced for all relevant risk factors and outcomes [33], the low incidence of RTLI in clinical and the long follow-up time needed for RTLI outcomes in NPC may make the research hard to implement. Second, we did not perform the external validation with independent data sets for generalization. The DCA and subgroup validation of different clinical factors used in this study, which enables the evaluation of clinical relevance in a traditional decision-analytic approach, justified that the identified radiomics signature and radiomics nomogram hold great potential for clinical application in RTLI outcome estimation. Third, the ROI of the TL was drawn manually, which is a time-consuming task and requires automated segmentation techniques in the near future. Finally, the dosimetric parameters included in this study were limited and not independent predictors of RTLI in the training set. In general, the feasibility of radiomics and clinical and dosimetric parameters to predict RTLI should be explored by future studies, especially prospective studies, with larger sample sizes at multicenter institutions.

In summary, we developed and validate a machine learning approach for predicting radiation-induced temporal lobe injury (RTLI) in patients with nasopharyngeal carcinoma (NPC) by pretreatment temporal lobe MRI. The identified radiomics signature has the potential to be used as a biomarker for risk stratification in RTLI. The radiomics nomogram described here, which well demonstrated the incremental value of the radiomics signature to other clinical-pathologic factors for accurate prediction of RTLI, further studies are required to explore the generalized utility of our model and apply our results to clinical application.

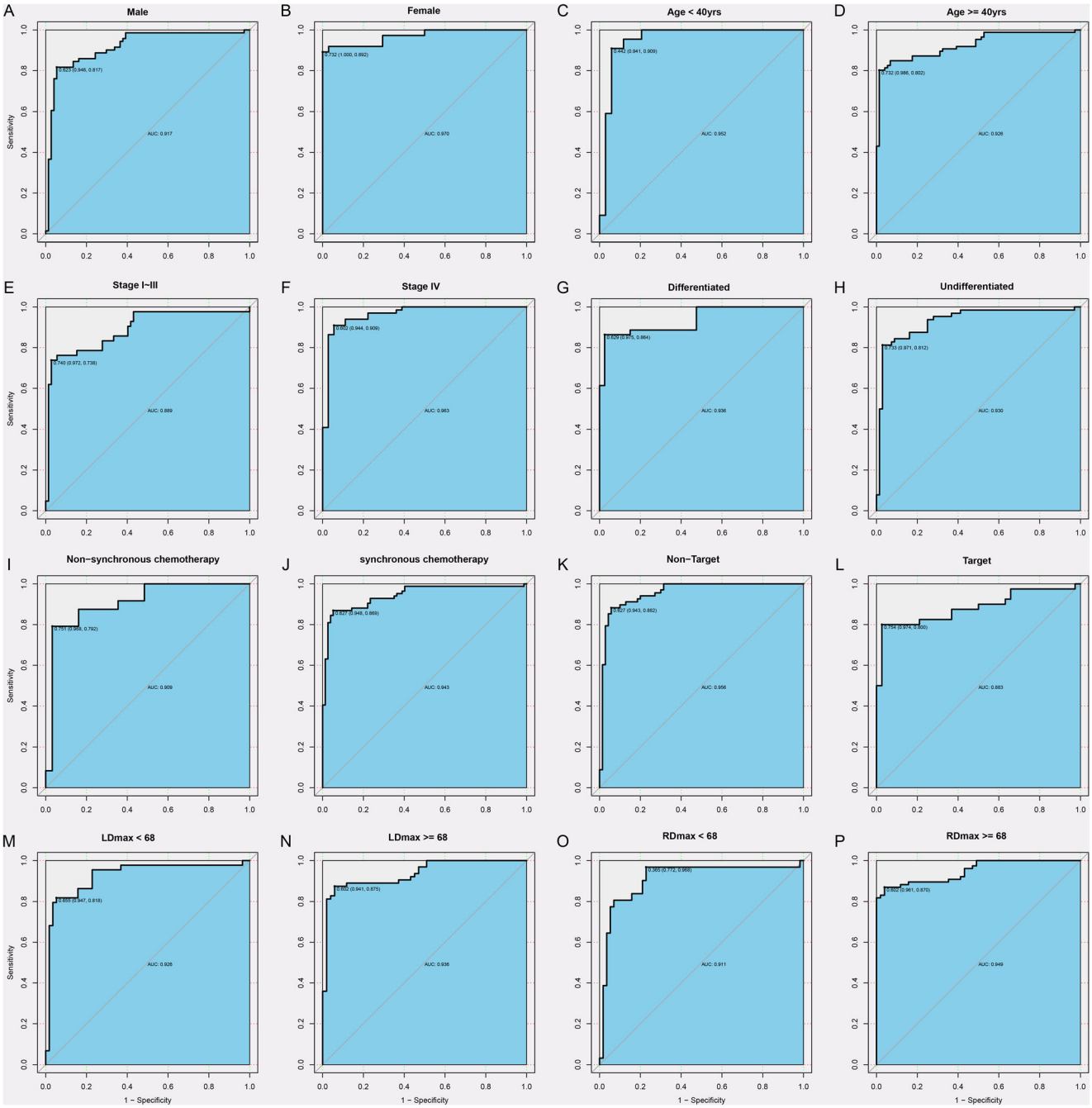

Fig. 6 The performances of clinical-radiomics model within different clinical-pathologic subgroups. ROC analysis with the AUC to evaluate the clinical-radiomics model as an independent biomarker in the following clinical-pathologic factors respectively: **a**, **b** gender (male or female); **c**, **d** age (< 40 or ≥ 40); **e**, **f** TNM stage (I–III or IV); **g**, **h** pathologic type (differentiated non-keratinizing, or undifferentiated non-keratinizing); **i**, **j** synchronous chemotherapy (untreated or treated); **k**, **l** targeted therapy (untreated or treated); **m**, **n** D_{max} of left temporal lobe (< 68 Gy or ≥ 68 Gy); **o**, **p** D_{max} of right temporal lobe (< 68 Gy or ≥ 68 Gy)

Supplementary Information The online version contains supplementary material available at https://doi.org/10.1007/s00330-022-08853-w.

Funding This study has received funding from the Non-profit Central Research Institute Fund of the Chinese Academy of Medical Sciences (2019XK320073).

Declarations

Guarantor The scientific guarantor of this publication is Dehong Luo.

Conflict of interest The authors of this manuscript declare no relationships with any companies, whose products or services may be related to the subject matter of the article.

Statistics and biometry One of the authors has significant statistical expertise.

Informed consent Written informed consent was waived by the Institutional Review Board.

Ethical approval Institutional Review Board approval was obtained.

Methodology
- retrospective
- diagnostic or prognostic study
- performed at one institution

References

1. Bray F, Ferlay J, Soerjomataram I, Siegel RL, Torre LA, Jemal A (2018) Global cancer statistics 2018: GLOBOCAN estimates of incidence and mortality worldwide for 36 cancers in 185 countries. CA Cancer J Clin 68:394–42
   Erratum in: CA Cancer J Clin. 2020;70:313
2. Pfister DG, Spencer S, Adelstein D et al (2020) Head and Neck Cancers, Version 2.2020, NCCN Clinical Practice Guidelines in Oncology. J Natl Compr Canc Netw 18:873–898
3. Lee AW, Law SC, Ng SH et al (1992) Retrospective analysis of nasopharyngeal carcinoma treated during 1976-1985: late complications following megavoltage irradiation. Br J Radiol 65:918–928
4. Liang SB, Wang Y, Hu XF et al (2017) Survival and toxicities of IMRT based on the RTOG protocols in patients with nasopharyngeal carcinoma from the endemic regions of China. J Cancer 8: 3718–3724
5. Su SF, Huang Y, Xiao WW et al (2012) Clinical and dosimetric characteristics of temporal lobe injury following intensity modulated radiotherapy of nasopharyngeal carcinoma. Radiother Oncol 104:312–316
6. Zhou GQ, Yu XL, Chen M et al (2013) Radiation-induced temporal lobe injury for nasopharyngeal carcinoma: a comparison of intensity-modulated radiotherapy and conventional two-dimensional radiotherapy. PLoS One 8:e67488
7. Lam TC, Wong FC, Leung TW, Ng SH, Tung SY (2012) Clinical outcomes of 174 nasopharyngeal carcinoma patients with radiation-induced temporal lobe necrosis. Int J Radiat Oncol Biol Phys 82: e57–e65
8. Abayomi OK (2002) Pathogenesis of cognitive decline following therapeutic irradiation for head and neck tumors. Acta Oncol 41: 346–351
9. Chen W, Qiu S, Li J et al (2015) Diffusion tensor imaging study on radiation-induced brain injury in nasopharyngeal carcinoma during and after radiotherapy. Tumori 101:487–490
10. Guan W, Xie K, Fan Y et al (2020) Development and validation of a nomogram for predicting radiation-Induced temporal lobe injury in nasopharyngeal carcinoma. Front Oncol 10:594494
11. Zeng L, Huang SM, Tian YM et al (2015) Normal tissue complication probability model for radiation-induced temporal lobe injury after intensity-modulated radiation therapy for nasopharyngeal carcinoma. Radiology 276:243–249
12. Huang J, Kong FF, Oei RW et al (2019) Dosimetric predictors of temporal lobe injury after intensity-modulated radiotherapy for T4 nasopharyngeal carcinoma: a competing risk study. Radiat Oncol 14:31
13. Lee AW, Cheng LO, Ng SH et al (1990) Magnetic resonance imaging in the clinical diagnosis of late temporal lobe necrosis following radiotherapy for nasopharyngeal carcinoma. Clin Radiol 42:24–31
14. Chen Q, Lv X, Zhang S et al (2020) Altered properties of brain white matter structural networks in patients with nasopharyngeal carcinoma after radiotherapy. Brain Imaging Behav 14:2745–2761
15. Wang HZ, Qiu SJ, Lv XF et al (2012) Diffusion tensor imaging and 1H-MRS study on radiation-induced brain injury after nasopharyngeal carcinoma radiotherapy. Clin Radiol 67:340–345
16. Yang J, Xu Z, Gao J et al (2018) Evaluation of early acute radiation-induced brain injury: Hybrid multifunctional MRI-based study. Magn Reson Imaging 54:101–108
17. Giraud P, Giraud P, Gasnier A et al (2019) Radiomics and machine learning for radiotherapy in head and neck cancers. Front Oncol 9:174
18. Mayerhoefer ME, Materka A, Langs G et al (2020) Introduction to Radiomics. J Nucl Med 61:488–495
19. Wang YX, King AD, Zhou H et al (2010) Evolution of radiation-induced brain injury: MR imaging-based study. Radiology 254: 210–218
20. Duane F, Aznar MC, Bartlett F et al (2017) A cardiac contouring atlas for radiotherapy. Radiother Oncol 122:416–422
21. Kim JH (2019) Multicollinearity and misleading statistical results. Korean J Anesthesiol 72:558–569
22. Thibault G, Fertil B, Navarro C et al (2009) Texture indexes and gray level size zone matrix. Application to cell nuclei classification. 10th International Conference on Pattern Recognition and Information Processing, PRIP 2009, Minsk, Belarus, pp 140–145
23. Amadasun M, King R (1989) Textural features corresponding to textural properties. IEEE Trans Syst Man Cybern 19(5):1264–1274
24. Tomaszewski MR, Gillies RJ (2021) The biological meaning of radiomic features. Radiology 298:505–516. https://doi.org/10.1148/radiol.2021202553 Erratum in: Radiology 2021;299:E256
25. Mori M, Passoni P, Incerti E et al (2017) Increased chemosensitivity and radiosensitivity of human breast cancer cell lines treated with novel functionalized single-walled carbon nanotubes. Oncol Lett 13:206–214
26. Jia Y, Weng Z, Wang C et al (2017) Increased chemosensitivity and radiosensitivity of human breast cancer cell lines treated with novel functionalized single-walled carbon nanotubes. Oncol Lett 13:206–214
27. Balentova S, Adamkov M (2015) Molecular, cellular and functional effects of radiation-induced brain injury: a review. Int J Mol Sci 16: 27796–27815
28. Hou J, Li H, Zeng B et al (2021) MRI-based radiomics nomogram for predicting temporal lobe injury after radiotherapy in nasopharyngeal carcinoma. Eur Radiol 32:1106–1114
29. Zhang B, Lian Z, Zhong L et al (2020) Machine-learning based MRI radiomics models for early detection of radiation-induced brain injury in nasopharyngeal carcinoma. BMC Cancer 20:502
30. Miller NR (2004) Radiation-induced optic neuropathy: still no treatment. Clin Experiment Ophthalmol 32:233–235
31. Chan YL, Leung SF, King AD, Choi PH, Metreweli C (1999) Late radiation injury to the temporal lobes: morphologic evaluation at MR imaging. Radiology 213:800–807
32. Bluemke DA, Moy L, Bredella MA et al (2020) Assessing radiology research on artificial intelligence: a brief guide for authors, reviewers, and readers-from the Radiology Editorial Board. Radiology 294:487–489
33. Moons KG, Altman DG, Reitsma JB et al (2015) Transparent Reporting of a multivariable prediction model for Individual Prognosis or Diagnosis (TRIPOD): explanation and elaboration. Ann Intern Med 162:W1–W73